DNA mold templated assembly of conductive gold nanowires

Bayrak, T.; Helmi, S.; Ye, J.; Kauert, D.; Kelling, J.; Schönherr, T.; Erbe, A.; Seidel, R.;

Originally published:

February 2018

Nano Letters 18(2018)3

DOI: https://doi.org/10.1021/acs.nanolett.8b00344

DNA mold templated assembly of conductive gold nanowires

Türkan Bayrak[†,‡,#], *Seham Helmi*[§,□,#], *Jingjing Ye*[‡,§,#], *Dominik Kauert*[§], *Jeffrey Kelling*[$], *Tommy Schönherr*[†], *Richard Weichelt*[&,‡], *Artur Erbe*[†,‡,*], *Ralf Seidel*[‡,§,*]

[†] Institute of Ion Beam Physics and Materials Research, Helmholtz-Zentrum Dresden-Rossendorf, 01328 Dresden, Germany

[‡] Cluster of Excellence Center for Advancing Electronics Dresden (cfaed), TU Dresden, 01062 Dresden, Germany

[§] Molecular Biophysics group, Peter Debye Institute for Soft Matter Physics, Universität Leipzig, 04103 Leipzig, Germany

[$]Department of Information Services and Computing, Helmholtz-Zentrum Dresden-Rossendorf, 01328 Dresden, Germany

[&]Institute of Physical Chemistry, TU Dresden, 01062 Dresden, Germany

[□] Present address: Department of Physics, University of Oxford, Oxford OX13PU, UK

[#] These authors contributed equally to the presented work

* Corresponding author contacts:

Artur Erbe: a.erbe@hzdr.de, Tel. +49 351 260 2366

Ralf Seidel: ralf.seidel@physik.uni-leipzig.de. Tel. +49 341 97 32501

ABSTRACT We introduce a new concept for the solution-based fabrication of conductive gold nanowires using DNA templates. To this end we employ DNA nanomolds inside which electroless gold deposition is initiated by site-specific attached seeds. Using programmable interfaces individual molds self-assemble into micrometer long mold superstructures. During subsequent internal gold deposition, the mold walls constrain the metal growth, such that highly homogeneous nanowires with 20-30 nm diameter are obtained. Wire contacting using electron beam lithography and electrical conductance characterization at temperatures between 4.2 K and room temperature demonstrate that metallic conducting wires were produced, though for part of the wires the conductance is limited by boundaries between gold grains. Using different mold designs, our synthesis scheme will in future allow the fabrication of complex metal structures with programmable shape.

KEYWORDS Metal nanowires, seeded growth, DNA metallization, DNA nanostructures, DNA template, nanoelectronics

The past decade has seen a boost in the field of DNA nanotechnology. A number of pioneering techniques[1-6] were developed that allow the self-assembly of large two- and three-dimensional DNA structures with complex shapes. The basis of these techniques are specific interactions between complementary DNA strands. By appropriate sequence design of the involved DNA molecules a desired structure can thus be obtained in a fully programmable, sequence-encoded manner. The beauty, the complexity[1-6] and the increased rigidity[7] of the down-to-the-atomic-level defined objects instantaneously motivated the usage of DNA nanostructures to assemble non-DNA materials in defined patterns. Examples include the arrangements of proteins[8], chemical[9] and photoactive groups[10, 11], the assembly of metal nanoparticles into plasmonic nanostructures[12-14] and the sculpting of lipid membranes.[15, 16]

DNA nanotechnology is particularly successful in generating soft nanostructures. However, many applications in "hard-matter nanotechnology" in particular in nanooptics and nanoelectronics require structures made from inorganic, e.g. metallic and semiconducting, rather than biological materials. Especially the low electrical conductance found in contacts to single DNA duplexes is detrimental for applications in nanoelectronics[17]. Therefore, it would be highly desirable, if one could "replace" the DNA structure atom by atom site-specifically with a material of choice to enable a programmable synthesis of inorganic nanostructures. Though a direct replacement will be practically impossible, the outlined idea inspired the usage of DNA as a template for inorganic material growth. Hereby the biomolecule would donate its shape to the growing material film. In first approaches, linear DNA molecules were metallized by so called electroless deposition, where first metal seeds are deposited on the molecule that are subsequently grown to more continuous structures. This way elongated metal particle assemblies could be fabricated.[18-20] Later, this concept could be extended to many different materials, including gold, silver, platinum, palladium, copper and cobalt.[21] With the advances in DNA

nanotechnology, rigid DNA template structures with more complex shapes became available enabling the growth of elongated wires[22], metal rings[23], junctions[24] and spheres[25] as well as structures consisting of two types of metals.[26] The deposited metal films were, however, not homogeneous and typically contained many distinct grains. This made the resulting structures either discontinuous[20] or inhomogeneous[27] depending on the amount of deposited material.

Nonetheless, wires produced this way were often found to conduct electric current when contacted either by electron-beam-lithography-fabricated electrodes[19, 28-32] or conductive AFM tips[33, 34]. Reported resistance values spanned several orders of magnitudes. Typically, the observed resistivities were significantly larger than expected for the respective metal forming the wire, indicating that grain boundaries can act as significant barriers. This was supported by recent temperature-dependent (4.2K to 293K) conductance measurements on DNA origami-based Au nanowires from our laboratory showing that tunneling, thermionic and hopping conduction mechanisms govern the conductance at low, intermediate and high temperature, respectively.[22] Also a recent study of 500 nm nanopillars, realized as multilayer-heterostructure of DNA origami tiles and Au nanoparticles, suggested tunneling or hopping conduction mechanism at room temperature.[28] In order to limit the number of grain boundaries, recently elongated Au nanorods were deposited in an aligned manner on DNA origami templates and connected using limited electroless Au-plating.[35] This provided resistance values for wires of 12 to 30 nm width in the range of 440 Ω to 37 MΩ with resistivities close to bulk gold for the wires with the highest conductances. This further supports the idea that grain boundaries due to inhomogeneous growth conditions appear to be one of the challenges in DNA-templated fabrication of metallic wires.

A key problem for the traditional external deposition on DNA templates is the lacking size-control for the particles that grow at the different positions along the DNA chain. This makes the methodology prone to inhomogeneities. Inspired by internal metal deposition schemes inside

protein shells[36, 37], we and others recently developed a DNA mold-based nanoparticle fabrication scheme[38, 39]. Here, the metal deposition occurs on a nucleation seed inside the cavity of a DNA origami mold, such that the mold wall influences the shape of the resulting particle. This way it was possible to synthesize gold and silver cuboids of different dimensions and shapes.

Here we extend the mold-based nanostructure fabrication scheme by coupling mold monomers into large linear mold superstructures (Figure 1). This enables the growth of highly homogeneous, µm-long nanowires with ~30 nm width that in part exhibit metallic conductance. To this end we assembled DNA molds using the DNA origami method[1, 2] from an 8064 nucleotide long single-stranded DNA scaffold and corresponding DNA staple oligomers (see Methods). The mold monomers had a 40 nm long tube-like shape with quadratic cross section[39]. Each side wall of the mold was composed from two layers of 10 parallel DNA helices of equal length (Figure 1) providing a total of 64 helices for the whole mold structure. Fabricated mold monomers were preloaded with 5 nm DNA-functionalized gold nanoparticles[40, 41] serving as seeds for the subsequent gold growth. They were attached within the molds via four complementary DNA capture strands extruding from the four cavity faces at the given binding position (Figure 1a).[39]

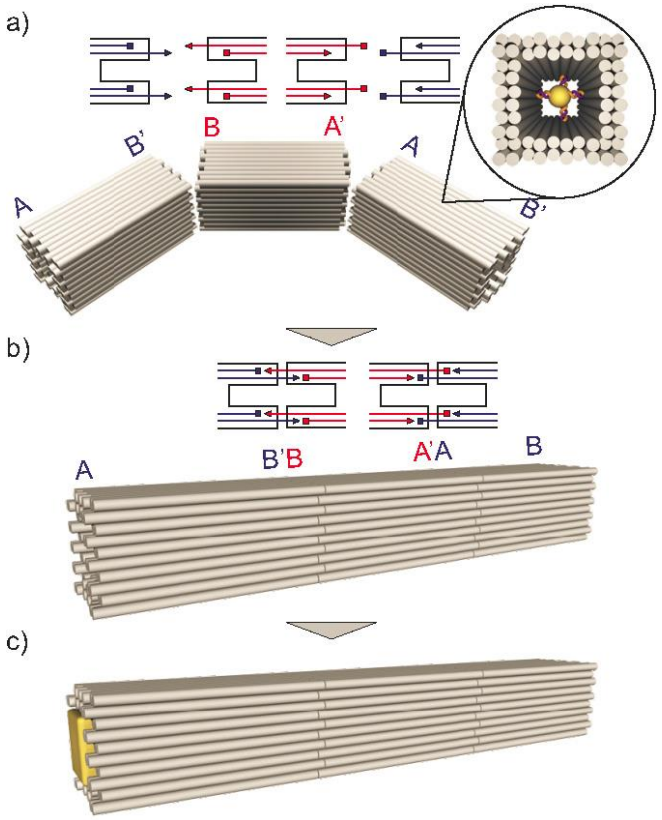

Figure 1. Scheme illustrating the mold-based gold nanowire a) Design scheme of the mold bricks with specifically interacting ends containing an internally attached 5 nm gold seed (see inset, upper right corner). Adhesion of mold ends is either obtained by protruding 5′-staple ends together with correspondingly recessed 3′-staple ends at the mold ends (A-A′ interface, see sketches in top row) or protruding 3′-staple ends together with recessed 5′-staple ends (B-B′ interface). b) Self-assembly of a long mold superstructure using two mold types each carrying an A or a B interface being complementary to the A′ or the B′ interface of the other mold type, respectively. c) Gold nanowire formation by metal deposition at the seeds inside the mold chain.

To allow the formation of long linear mold superstructures via sequential docking of mold monomers, we extended or shortened the staples at the DNA helix ends (further called end staples) by two nucleotides such that the 2-nt extensions of one mold could invade into the other mold and hybridize with its scaffold (Figures 1a and 1b).

The mold geometry with helices of identical length is asymmetric with respect to its ends. If we call one mold end the head and the other end the tail side, then a particular DNA helix that is recessed at the head side is extended at the tail side (and vice versa), which results in a symmetry break. Thus, when mold ends bind in a head-to-tail fashion, docking can be obtained at all 64 helix ends leaving no gap at the interface. However, for head-to-head or tail-to-tail binding a significantly lower number of docking helices is obtained (44 or 36, respectively). To obtain "neat-less", i.e. gap-free, mold superstructures we therefore designed end staples to support head-to-tail binding. We prepared two different types of interfaces: interface A-A′ for which end staples were extended by 2 nt at the 5′-ends and correspondingly recessed at the 3′-ends as well as interface B-B′ with recessed 5′-ends and extended 3′-ends (Figure 1a). Here, A and B denote the head side of the mold and A′ and B′ the complementary side on a mold tail side, respectively.

For the assembly of linear mold chains a single interface, e.g. monomers with A-A′ ends would suffice. In this case mold chains would already form during origami hybridization, which would, however, inhibit the loading of the molds with gold seeds at internal sites. We therefore designed two different mold monomers – one with AB′ ends and the other with BA′ ends. While each mold type would be monomeric alone, their mixing should result in the desired chain formation (Figure 1-2).

Following the outlined approach, we assembled AB′ and BA′ molds, loaded them with gold nanoparticle seeds and subjected them to TEM imaging (Figure 2a, Supporting information, Figure S1). In contrast to our expectations, both monomers alone formed extended linear, partially staggered, chains, which in turn led to poor decoration with seeds. We hypothesized that due to the large number of "attractive" ends (all 64 helix ends contained 2 nt recessions/extensions) mold monomers could bind to themselves forming non-desired head-to-head and tail-to-tail interactions. Apparently, the presence of mismatches between staple

extension and scaffold did not lower the affinity between single helix ends sufficiently to prevent unspecific binding.

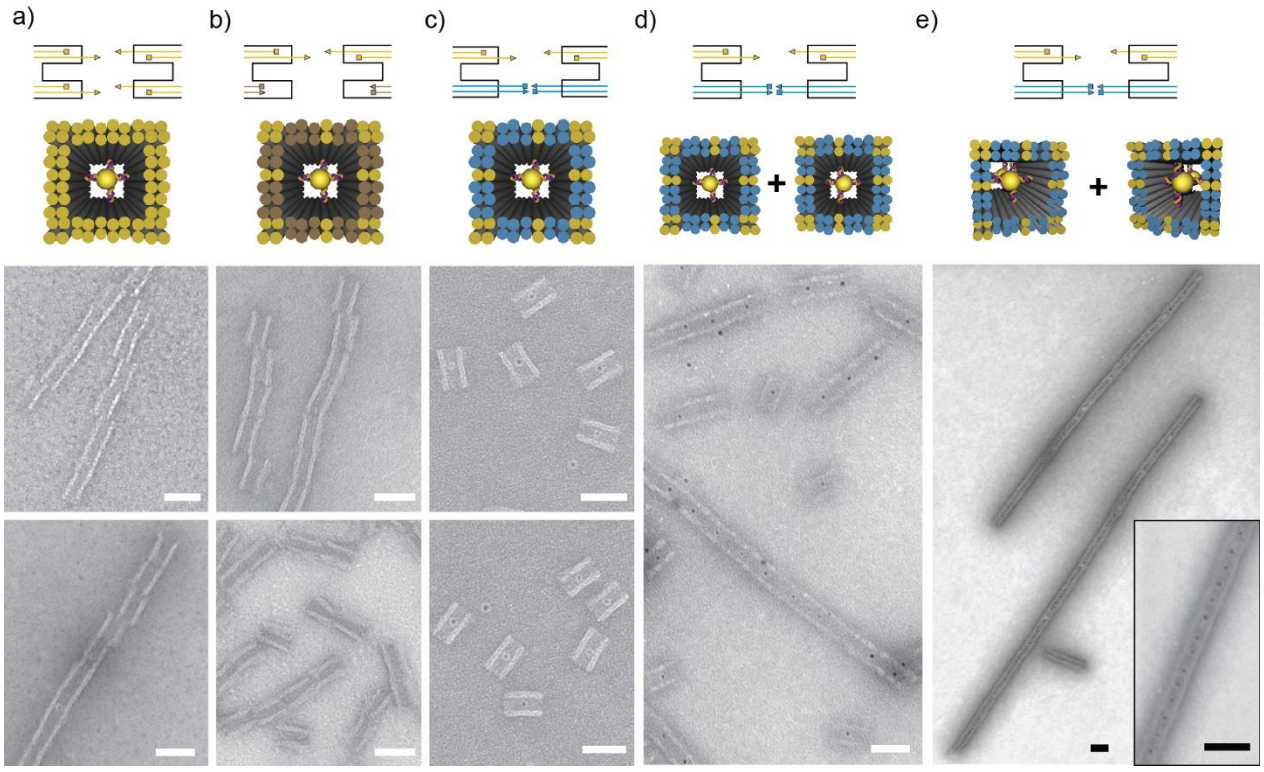

Figure 2. Fine-tuning the specificity of adhesive mold ends. (a-c) Type of staple ends used and their positions on the 3D model (upper row) as well as corresponding TEM images of the AB′ and BA′ mold monomers. Tested were a) attractive ends only (in yellow), (b) attractive ends together with non-attractive ends (in gray, obtained by omitting ends staples) and (c) attractive and repulsive ends (blue, obtained by 6 nt non-complementary 5′-staple overhangs). (d) Mixing AB′ and BA′ mold monomers comprising attractive and repulsive end staples (as in c) results in mold oligomer formation. (e) Using optimized multimerization conditions, long linear mold chains are obtained. Preloading of the monomers with two seeds at high decoration efficiency results in a homogeneous loading of seeds inside the mold superstructure (see Inset). The scale bars correspond to 50 nm.

To suppress unspecific interactions, the number of attractive helix ends was reduced by omitting end staples at some of the helix ends, which are in the following called non-attractive ends. Here the scaffold forms a dangling loop. For 16 to 24 attractive ends with the remaining ends being non-attractive, considerable unspecific interactions between mold monomers were observed nonetheless (Figure 2b, Supporting information, Figure S1). To further reduce unspecific binding, repulsive interactions between helix ends were incorporated. To this end, the previously non-attractive ends were made repulsive by extending the end staples at these positions by 6 nt, both for 5' and 3' ends (see sketch in Figure 2c). The steric clash between these dangling ends should introduce an energetic penalty compared to the non-attractive end configuration. In agreement with this expectation, TEM imaging revealed the monomeric nature of molds containing up to 24 attractive helix ends (Figure 2c, Supporting information, Figure S1). These monomers exhibited a high seed decoration efficiency, since gold nanoparticles could freely enter the mold ends.

We next tested whether the optimized molds with attractive and repulsive ends could form specific interactions by mixing seed decorated AB′ and BA′ monomers. While molds with 16 and 20 attractive helix ends remained mostly monomeric (Supporting information, Figure S1), molds with 24 attractive ends supported the formation of linear oligomeric mold assemblies already after 10 min of incubation (Figure 2d). To prepare long mold chains for subsequent metallization we carried out the following optimizations: (i) addition of 2 seeds per mold monomer to avoid interruption of gold wire in case of missing seeds, (ii) chain formation overnight to obtain long assemblies and (iii) polyethylene glycol (PEG) precipitation[42] after chain formation to remove unbound gold seeds. All together, these optimizations yielded µm-long linear mold chains containing evenly 20-nm spaced gold seeds with 96 ± 2% decoration efficiency (Figure 2e).

To fabricate gold nanowires, the linear mold superstructures were used in a previously established seeded growth procedure.[39] Mold chains were premixed with the reducing agent hydroxylamine. Subsequently, a solution of the gold precursor $H[AuCl_4]$ was quickly injected into the rapidly stirred solution. The reaction self-terminated due to the consumption of $H[AuCl_4]$ after ~1 min as judged from color changes of the solution. TEM and SEM imaging revealed a homogenous gold deposition at all seeds (Figure 3). The lengths of the grown structures were in the μm-range (Supporting information, Figure S2). At low amounts of precursor the grown gold particles still remained well separated (Figure 3a), while at larger amounts of precursor the grown particles appeared more and more connected to each other (Figures 3b, c, Supporting information, Figure S3). At the largest precursor concentration the particles formed quasi-continuous μm-long wires that were occasionally interrupted by smaller gaps (Figures 3c,d, Supporting information, Figure S4). These structures were stable in solution for several days. Only at larger precursor concentrations aggregation occurred. We note that the highly homogeneous particle growth and the stability of the wires was only achieved when the seed-loaded mold chains were subjected to the PEG precipitation before metallization. This was most likely due to residual PEG traces, since PEG is also used as a surfactant in nanoparticle synthesis[43]. The resulting nanowires (Fig. 3d) had diameters of 32 ± 3 nm. Despite occasional gaps, these wires were of excellent homogeneity compared to other DNA templated metal structures. Thus, the mold-assisted growth of metal nanoparticles can be successfully transferred to large mold superstructures.

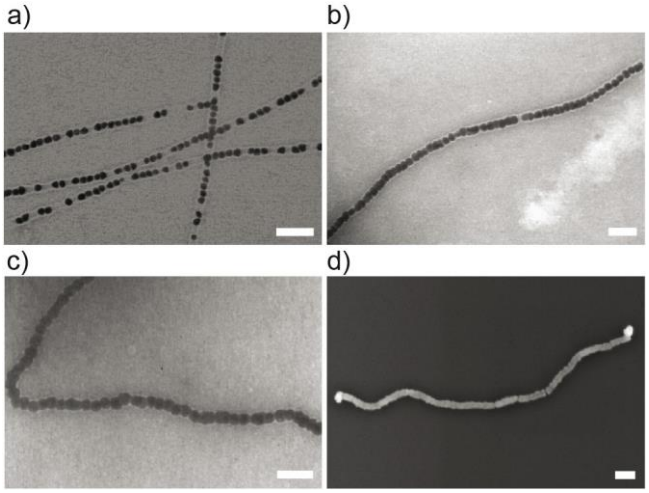

Figure 3. Gold nanowires obtained by gold deposition within the seed decorated linear mold superstructures. TEM images of the obtained structures for different relative amounts of gold precursor are shown: (a) 1-fold, (b) 2-fold and (c) 4-fold $H[AuCl_4]$. (d) SEM image of a gold nanowire on a SiO_2 support grown with 4-fold $H[AuCl_4]$. The scale bars correspond to 50 nm.

In order to reveal which role residual gaps are playing and whether the wires can exhibit metal-like conductance, we investigated the electrical transport properties of several fabricated nanowires with 110 to 1000 nm in length. The electrical contacting of individual DNA origami mold-based gold nanowires was performed in three steps: (i) Using electron beam lithography, 45 contact areas (in three parallel arrays) were patterned on top of SiO_2 substrates containing the adsorbed gold nanowires. Each contact area had four 90 µm x 90 µm Au contact pads and 144 alignment marks arranged in a square lattice with 8 µm distance between neighboring marks (Figure 4a). (ii) Using scanning electron microscopy the coordinates of the individual wires relative to the alignment marks were recorded (Figure 4b). (iii) The recorded locations of the nanowires were used to obtain corresponding e-beam exposure positions in order to place electrical contacts on the nanowires. This procedure allowed to write four electrodes even on a 600 nm long nanowire (Figure 4c). Overall the wires well adhered to the substrate, such that they

retained their shape during the lithography and the solvent based ultrasonic lift-off process, as confirmed by SEM imaging.

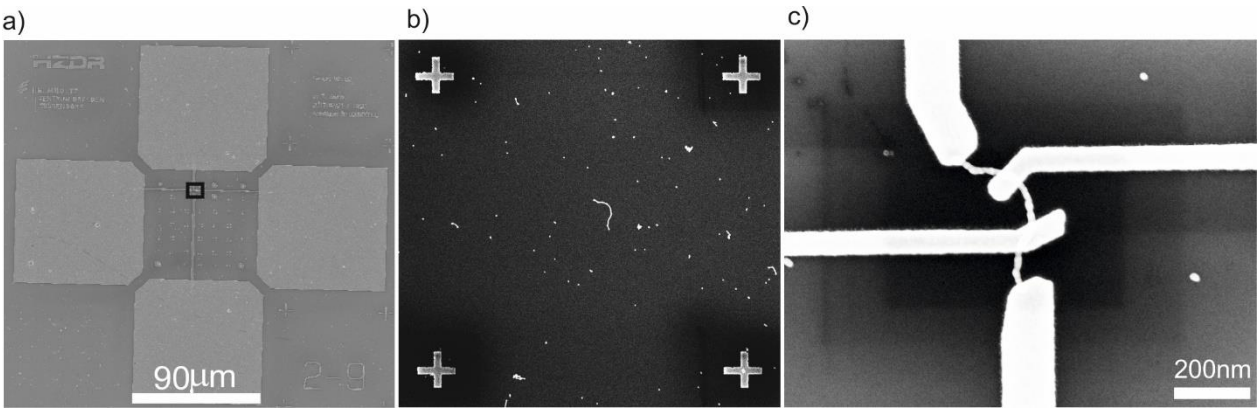

Figure 4. Electrical contacting of mold-templated nanowires. (a) SEM images of one out of 45 contact areas comprising four contact pads. Contact pads were fabricated on SiO_2 substrates containing the adsorbed gold nanowires. In between the electrodes 144 alignment markers arranged in a square lattice defined 36 "writing" fields of 8 x 8 µm size. (b) Enlarged view into a single writing field (corresponding to the black square in a) containing a 600 nm long gold nanowire. (c) The gold nanowire shown in b after contact writing. Each contact to the wire connects to one of the four contact pads shown in a.

Two-terminal current-voltage (*I-V*) measurements were performed on 22 individual wires. The measured resistance values at room temperature (RT, i.e. 293K) including the contact resistance between EBL-patterned gold electrodes and nanowires were between 90 Ω and 30 GΩ without showing a clear length dependence (Figure 5).

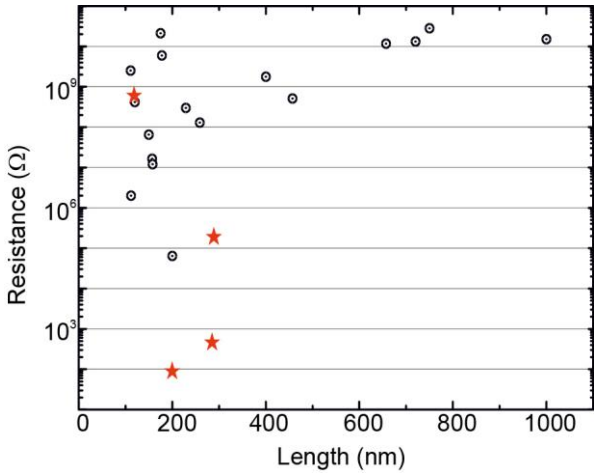

Figure 5. Resistance values as function of length for the characterized gold nanowires. Wires chosen for temperature-dependent measurements are shown by a star-shaped symbol.

The limited resolution of SEM imaging on the SiO_2 substrates did not allow to correlate the measured resistance with the wire morphology (Supporting information, Figure S5). Therefore, to understand the large variation in resistance values, we measured the temperature dependence of the charge transport of two highly conductive nanowires (labelled CW-1 and CW-2 with RT resistances of 90±5 Ω and 460±10 Ω) as well as two highly resistive nanowires (labelled RW-1 and RW-2 with RT resistances of 190±5 kΩ and 690±5 MΩ). The inset of figure 6a) depicts a nanowire with a length of 800 nm, which was contacted by four terminal gold contacts. SEM imaging revealed 13-15 nm gaps between the contact points 2 and 3 as well as 3 and 4 leading to insulating behavior in *I-V* measurements (see Supporting information, Figure S6). A high conductance was found for the wire segment between contacts 1 and 2 (CW-1). The *I-V* characteristics of CW-1 (200 nm length, 40 nm widths) was linear throughout the considered temperature range between 4.2K and RT (see Figure 6b and Supporting information, Figure S7a). This indicates an ohmic behavior of the nanowire itself as well as its contacts. The resistance of the wire was weakly decreasing with temperature from 90 Ω at 293K to 50 Ω at 4.2K as expected for a metallic wire. A qualitatively similar behavior was observed for the 285 nm long nanowire

CW-2 with 30 nm average width (see Figure 6b and Supporting information, Figure S7b) for which resistances of 460 and 420 Ω at 293 and 4.2 K were measured, respectively.

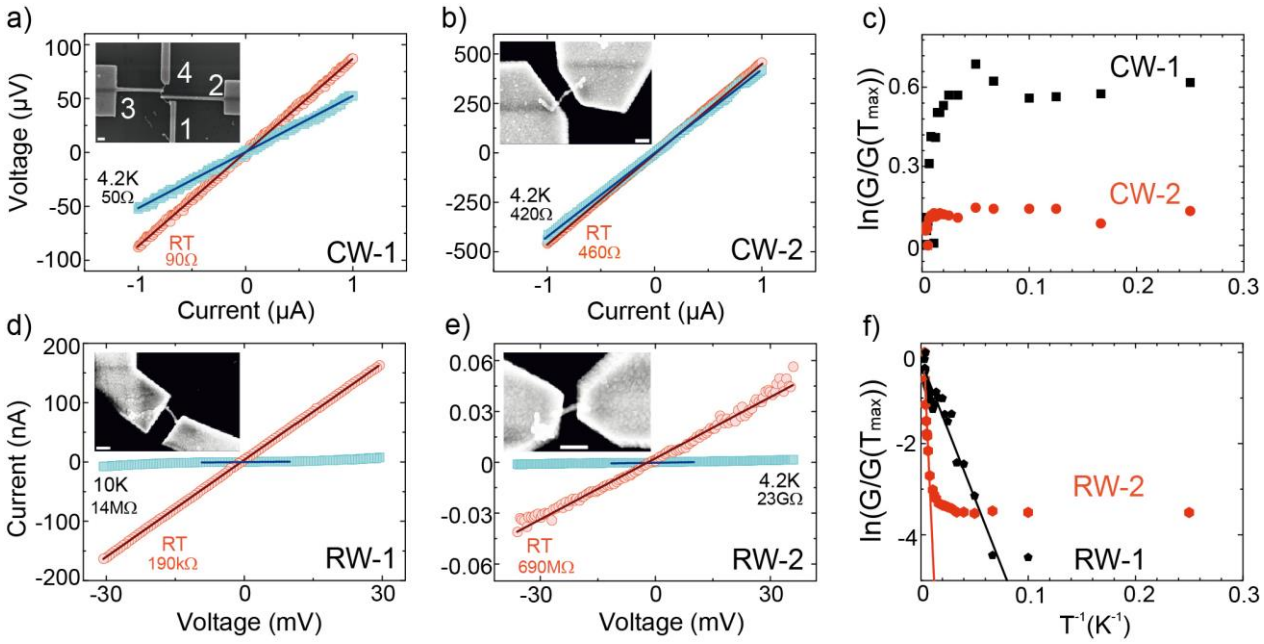

Figure 6. *I-V* characteristics of the different nanowires measured at the temperatures of 4.2 and 293 K. SEM inset images show the nanowires after contacting (scale bars are 200 nm). (a,b) *I-V* curves for the highly conductive wires CW-1 and CW-2 obtained by sourcing the current and measuring the voltage drop across the wire. Resistance values shown next to the curves were obtained from linear fits (solid lines). (c) Normalized natural logarithm of the conductance values as a function of T^{-1} for CW-1 and CW-2. (d,e) *I-V* curves for the resistive wires RW-1 and RW-2 obtained by applying a voltage bias and measuring the resulting current. (f) Normalized natural logarithm of the conductance values as a function of T^{-1} for RW-1 and RW-2 (filled circles). Exponential fits to the data in a selected temperature range are shown as solid lines.

Temperature dependent *I-V* measurements on the more resistive nanowires RW-1 (290 nm length, 36 nm width) and RW-2 (115 nm length, 39 nm width) revealed linear behavior at RT (Figures 6d and 6e). However, at low temperatures (50K to 4K), the *I-V* curves became non-

linear in between -30mV and +30mV (Supporting information, Figure S7). Therefore, resistance values were calculated from the slope of the linear part of the curves (-10 mV to 10 mV). The resistance was strongly temperature dependent for both wires; it increased for RW-1 from 190 kΩ at RT to 14 MΩ at 10 K and for RW-2 from 700 MΩ at RT to 23 GΩ at 4K. Thus, both wires did not show metallic conductance behavior.

To better understand the nature of the charge transport in these nanowires, we plotted the normalized natural logarithm of the conductance $\ln[G/G(T_{max})]$ as function of the reciprocal temperature (T^{-1}). The conductance of both CW-1 and CW-2 increased mildly with decreasing temperature as discussed above (Figure 6c). Saturation of the conductance at low temperatures (4.2K to 20K) was observed in CW-1 and CW-2. In contrast, the conductance of the resistive nanowires RW-1 and RW-2 decreased strongly, initially in an exponential fashion with the reciprocal temperature (Figure 6f). While RW-1 exhibited an exponential decrease over the whole temperature range, the conductance of RW-2 saturated for temperatures below 30 K.

An exponential conductance decrease indicates a thermally activated hopping mechanism for the charge transport, e.g. due to low conductance barriers in between conductive wire segments. Here, the conductance is governed by the activation energy E_a necessary to overcome the barrier according to $G \sim \exp(-E_a/k_BT)$, where k_B is the Boltzmann constant.[44-46]

The activation energies of the wires were obtained from the slope of the linear sections in the conductance yielding 5 ± 0.5 meV for RW-1 (temperature range from 10K to RT) and 45 ± 5 meV for the more resistive wire RW-2 (temperature range from 70K to RT). While a hopping mechanism seems to dominate the conduction of RW-1 at all temperatures, hopping conductivity is observed for RW-2 only at high temperatures. At low temperatures, between 4K and 30 K, the independence of the conductance of RW-2 on the temperature suggests that direct tunneling of

electrons through an energy barrier is the dominant mechanism in this regime. For temperatures in between the tunneling and the hopping regime (30 K to 70 K) a thermionic conduction mechanism comes into play[21] due to decreases in the effective barrier height and the excitation of more electrons.

In summary, we successfully demonstrated the fabrication of highly homogeneous and conductive nanowires using DNA molds. An important step was herein the fine-tuning of the specificity of the mold-mold interactions using attractive and repulsive ssDNA overhangs. Only this way molds of a given type stayed monomeric and could thus be efficiently loaded with gold nanoparticle seeds. Mixing two mold types with like-wise attractive interfaces resulted in the formation of linear mold superstructures being hundreds of nanometers long and comprising dozens of monomers. The subsequent gold deposition at the seeds produced nanowire structures that consisted of nearly perfectly aligned gold nanoparticles of homogeneous size. This demonstrates, that the mold-assisted growth of metal nanoparticles can be applied to large superstructures. Our approach represents thus a new way to DNA-templated nanostructure fabrication.

At elevated amounts of deposited gold the grown nanoparticles became connected to each other, such that the resulting structures became quasi-continuous. To verify whether actual gold-gold contacts between the particles had been established, we employed temperature-dependent conductance measurements enabled by high-precision contacting of the wires using electron beam lithography. These characterizations provided diverging results. A small part of the wires exhibited high metal-like conductivity, verifying that metallic gold-gold contacts could be successfully formed over 20 to 30 contiguous particle boundaries (being spaced by 20 nm). This is remarkable, since only very recently high conductivities of DNA templated gold structures

were achieved using long gold nanorods with much fewer interfaces and a surface based metallization procedure.[35]

Establishing metallic contacts at the particle-particle interfaces still remains a critical factor, since many of the tested wires exhibited significantly reduced conductance values. Comprehensive temperature-dependent characterization of two more resistive wires revealed that the charge transport was dominated by a single effective energy barrier reflected by the single exponential decrease of the conductivity with reciprocal temperature. This suggests that the charge transport was dominated by a single non-metallic inter-particle interface that needed to be overcome by hopping at higher temperatures. The width of such non-metallic gaps was presumably in the low nanometer range supported by the observation of tunneling dominating the charge transport at low temperatures for one of the tested wires.

Future work will focus on improving the perfection of the obtained wires by increasing the yield from establishing metallic inter-particle contacts. Nonetheless, our results represent a considerable advancement in DNA-templated fabrication of electronic structure regarding the homogeneity and the potentially high conductivity of the obtained structures. Beyond that our approach, based on large DNA mold superstructures, opens a versatile route for self-assembly-based device fabrication. Using molds with different geometries (e.g. different diameters, additional docking sites, junctions) and specific interfaces as well as different materials should enable the fabrication of whole devices including gate electrodes and even device networks.

Methods

DNA-origami design, assembly, and analysis. The DNA origami molds (Supporting information, Figures S8 and S9) were designed using CaDNAno[47] comprising parallel helices arranged in a square lattice.[48] Reverse-phase cartridge purified oligonucleotides for the DNA origami objects were purchased from Eurofins MWG Operon. Single-stranded p8064 scaffold DNA was purchased from tilibit nanosystems (Garching, Germany). The one-pot assembly reaction was performed as follows: 10 nM scaffold p8064 was mixed in folding buffer containing 5 mM Tris-HCl, 1 mM EDTA and 11 mM $MgCl_2$ (pH 8.0) with unpurified staple strands and capture strands in a molar ratio of 1:10:1 (per individual sequence). The reaction was heated to 80°C for 5 min, and cooled to 25°C over 15 h using a non-linear temperature ramp with the slowest temperature decrease occurring between 55°C to 45°C. The folded objects were investigated with gel-electrophoresis (1% agarose gel, 0.5x TBE, 11 mM $MgCl_2$, 3.5 V/cm). Subsequently, the molds were purified using precipitation with polyethylene glycol to remove excess staples[42]. For TEM imaging, 2-3 µl of a diluted origami sample solution (1-2 nM) was applied to glow-discharged carbon-coated grids. The sample was subsequently stained using a filtered 2% solution of uranyl formate in 5 mM NaOH for 2 min. TEM imaging was performed in a Zeiss Libra 120 or a Phillips CM200 Ultra Twin transmission electron microscope at 80 kV or 120 kV, respectively.

Decoration of DNA molds with gold nanoparticle seeds. 5 nm AuNPs (Sigma-Aldrich) were densely coated with 15 nt poly-thymidine oligonucleotides carrying a 5'-thiol modification as described before using the method of salt aging.[39, 40, 49] The particle concentration was estimated from the absorbance at 520 nm. DNA-functionalized gold nanoparticles were mixed with the purified DNA origami molds in the presence of 300 mM NaCl at a molar ratio of 3:1 or 6:1 for molds with one or two seed binding sites, respectively. The mixture was slowly heated to 40°C

and afterwards cooled down to 23°C over a duration of 5 h to allow hybridization of the AuNPs with the complementary capture strands on the mold.

Formation of linear mold superstructures. Two types of mold monomers (AB´and BA`) were designed that only allow specific head-to-tail binding to the other monomer type (see Supplementary information, Figures S8 and S9 for the design details of the mold ends). After preloading with seeds both monomers were mixed in a 1:1 molar ratio and incubated for up to 24 h followed by a precipitation with PEG to remove excess seeds.

Seeded-growth of gold within mold superstructures. The concentration of the mold superstructures was adjusted with folding buffer (see above), such that 1 nM mold monomers were present in solution, and hydroxyl amine (NH_2OH) was added at a 6-fold molar access over the subsequently added gold precursor. The gold growth was initiated by injecting 1x, 2x or 4x of 0.9 µl of 25 mM $H[AuCl_4]$ into 100 µl final volume of the NH_2OH containing mold solution[39]. During growth the solution was vigorously stirred and after 1 min the grown wires were deposited on TEM grids or SiO_2 substrates.

Deposition of the gold nanowires on wafer substrates

Grown gold nanowires were deposited on p-doped Si/SiO_2 (300 nm oxide layer) wafer substrates diced into 1x1cm^2 squares. The surface was treated with an O_2 plasma (PICO, Diener Electronic-Plasma Surface Technology) at 7sccm O_2 and a power of 240W for 3min to make the hydrophobic surface more hydrophilic (see Supporting Information, Figure S10). The sample was rinsed with ethanol (20s) and pure-membrane water (20s). Subsequently, 20 µl of the nanowire sample were placed on the wafer surface for 1h. Afterwards, the substrate was dipped in a 1:1 mixture of ethanol and deionized water for 30 s. To remove the organic DNA layer around the nanowires, the sample was again subjected to an O_2 plasma at 7sccm O_2 and 300W for 30 min.

Electron beam lithography and electrical measurements

The electrical contact pads and markers were fabricated using electron beam lithography (RAITH e-line Plus). ZEP520 electron beam resist was spin coated on the samples and baked at 150°C for 10 min. The resist was exposed at 35μC/cm2 area dose to write contact pads, markers and small contacts, respectively. The resist was developed in n-Amyl acetate for 90s and subsequently in isopropanol for 30 s. A 5 nm Ti adhesion layer followed by a 100 nm gold layer were deposited at 0.2Å/s and 2Å/s with e-beam evaporation (Bestec UHV Evaporation Tool). Lift-off was performed by immersion in ZDMAC (Dimethylacetamide) and subsequent washing with IPA, followed by drying in a N_2-stream. Electrical measurements were carried out using a semiconductor parameter analyzer (Agilent 4156-C) in vacuum (10^{-5} mbar) and in the dark using two probes. A Helium flow cryostat system was used for temperature dependent electrical measurements. The samples were cooled down to 4.2K and measurements were performed while heating up. I-V measurements were performed by sweeping of the voltage (0 to 30mV and 0 to -30mV) or the current (0 to 1μA and 0 to -1μA) for resistive or conductive wires, respectively. The resistances or conductances of the were determined by least-squares fitting of a linear function to the measured V-I or I-V curves, respectively. For wires which showed non-linear I-V relations at low temperatures (RW-1 and RW-2), we determined the zero-bias resistance (conductance) as the slope of the curve at the inflection point near zero current (voltage).

ASSOCIATED CONTENT

Supporting Information. Additional electron-microscopy micrographs, design files for the origami mold construction as well as comprehensive data sets of the electric characterization of the wires. This material is available free of charge via the Internet at http://pubs.acs.org.

AUTHOR INFORMATION

Corresponding Authors

Artur Erbe, Nanotransport group, Institute of Ion Beam Physics and Materials Research, Helmholtz-Zentrum Dresden – Rossendorf, 01328 Dresden, Germany, Tel.: +49 351 260 2366, E-mail address: a.erbe@hzdr.de

Ralf Seidel, Molecular Biophysics group, Peter Debye Institute for Soft Matter Physics, Universität Leipzig, 04103 Leipzig, Germany, Tel.: +49 341 97 32501, E-mail address: ralf.seidel@uni-leipzig.de

Present Addresses

 Present address: Department of Physics, University of Oxford, Oxford OX13PU, UK

Funding Sources

This work was supported by the Deutsche Forschungsgemeinschaft within the Cluster of Excellence Center for Advancing Electronics Dresden (cfaed/TU Dresden) as well as grant SE 1646/8-1 to R.S. and by the Helmholtz Association through IHRS for Nanoelectronic Networks NanoNet (VH-KO-606).

ACKNOWLEDGMENT

We gratefully acknowledge Martin Bähler, Oliver Oeckler, Roger Gläser, Marius Grundmann, Jörg Lenzner, Markus Löffler and the Dresden Center for Nanoanalysis for access, training and support with respect to TEM and SEM imaging. We furthermore acknowledge Matthias Krause and Angela Schneider and Claudia Neisser for their help with and access to the Drop Shape Analysis System and the helium flow for the cryostat. We would like to thank Peter Zahn for useful discussions on the data of the electrical measurements.

REFERENCES

(1) Rothemund, P. W. K. Folding DNA to create nanoscale shapes and patterns. *Nature* **2006**, *440*, 297–302.

(2) Douglas, S. M.; Dietz, H.; Liedl, T.; Högberg, B.; Graf, F.; Shih, W. M. Self-assembly of DNA into nanoscale three-dimensional shapes. *Nature* **2009**, *459*, 414–418.

(3) Seeman, N. C. Nanomaterials based on DNA. *Annu. Rev. Biochem.* **2010**, *79*, 65–87.

(4) Han, D.; Pal, S.; Nangreave, J.; Deng, Z.; Liu, Y.; Yan, H. DNA origami with complex curvatures in three-dimensional space. *Science* **2011**, *332*, 342–346.

(5) Wei, B.; Dai, M.; Yin, P. Complex shapes self-assembled from single-stranded DNA tiles. *Nature* **2012**, *485*, 623–626.

(6) Benson, E.; Mohammed, A.; Gardell, J.; Masich, S.; Czeizler, E.; Orponen, P.; Högberg, B. DNA rendering of polyhedral meshes at the nanoscale. *Nature* **2015**, *523*, 441–444.

(7) Kauert, D. J.; Kurth, T.; Liedl, T.; Seidel, R. Direct mechanical measurements reveal the material properties of three-dimensional DNA origami. *Nano Lett.* **2011**, *11*, 5558–5563.

(8) Mikkilä, J.; Eskelinen, A.-P.; Niemelä, E. H.; Linko, V.; Frilander, M. J.; Törmä, P.; Kostiainen, M. A. Virus-encapsulated DNA origami nanostructures for cellular delivery. *Nano Lett.* **2014**, *14*, 2196–2200.

(9) Voigt, N. V.; Tørring, T.; Rotaru, A.; Jacobsen, M. F.; Ravnsbaek, J. B.; Subramani, R.; Mamdouh, W.; Kjems, J.; Mokhir, A.; Besenbacher, F.; Gothelf, K. V. Single-molecule chemical reactions on DNA origami. *Nat. Nanotechnol.* **2010**, *5*, 200–203.

(10) Hemmig, E. A.; Creatore, C.; Wünsch, B.; Hecker, L.; Mair, P.; Parker, M. A.; Emmott, S.; Tinnefeld, P.; Keyser, U. F.; Chin, A. W. Programming Light-Harvesting Efficiency Using DNA Origami. *Nano Lett.* **2016**, *16*, 2369–2374.

(11) Steinhauer, C.; Jungmann, R.; Sobey, T. L.; Simmel, F. C.; Tinnefeld, P. DNA origami as a nanoscopic ruler for super-resolution microscopy. *Angew. Chem. Int. Ed. Engl.* **2009**, *48*, 8870–8873.

(12) Gür, F. N.; Schwarz, F. W.; Ye, J.; Diez, S.; Schmidt, T. L. Toward Self-Assembled Plasmonic Devices: High-Yield Arrangement of Gold Nanoparticles on DNA Origami Templates. *ACS Nano* **2016**, *10*, 5374–5382.

(13) Thacker, V. V.; Herrmann, L. O.; Sigle, D. O.; Zhang, T.; Liedl, T.; Baumberg, J. J.; Keyser, U. F. DNA origami based assembly of gold nanoparticle dimers for surface-enhanced Raman scattering. *Nat. Commun.* **2014**, *5*, 3448.

(14) Kuzyk, A.; Schreiber, R.; Fan, Z.; Pardatscher, G.; Roller, E.-M.; Högele, A.; Simmel, F. C.; Govorov, A. O.; Liedl, T. DNA-based self-assembly of chiral plasmonic nanostructures with tailored optical response. *Nature* **2012**, *483*, 311–314.

(15) Yang, Y.; Wang, J.; Shigematsu, H.; Xu, W.; Shih, W. M.; Rothman, J. E.; Lin, C. Self-assembly of size-controlled liposomes on DNA nanotemplates. *Nat. Chem.* **2016**, *8*, 476–483.

(16) Czogalla, A.; Kauert, D. J.; Franquelim, H. G.; Uzunova, V.; Zhang, Y.; Seidel, R.; Schwille, P. Amphipathic DNA origami nanoparticles to scaffold and deform lipid membrane vesicles. *Angew. Chem. Int. Ed.* **2015**, *54*, 6501–6505.

(17) Livshits, G. I.; Stern, A.; Rotem, D.; Borovok, N.; Eidelshtein, G.; Migliore, A.; Penzo, E.; Wind, S. J.; Di Felice, R.; Skourtis, S. S.; Cuevas, J. C.; Gurevich, L.; Kotlyar, A. B.; Porath, D. Long-range charge transport in single G-quadruplex DNA molecules. *Nat. Nanotechnol.* **2014**, *9*, 1040–1046.

(18) Seidel, R.; Ciacchi, L. C.; Weigel, M.; Pompe, W.; Mertig, M. Synthesis of platinum cluster chains on DNA templates: Conditions for a template-controlled cluster growth. *J. Phys. Chem. B* **2004**, *108*, 10801–10811.

(19) Braun, E.; Eichen, Y.; Sivan, U.; Ben-Yoseph, G. DNA-templated assembly and electrode attachment of a conducting silver wire. *Nature* **1998**, *391*, 775–778.

(20) Mertig, M.; Ciacchi, L. C.; Seidel, R.; Pompe, W.; De Vita, A. DNA as a selective metallization template. *Nano Lett.* **2002**, *2*, 841–844.

(21) Wirges, C. T.; Timper, J.; Fischler, M.; Sologubenko, A. S.; Mayer, J.; Simon, U.; Carell, T. Controlled nucleation of DNA metallization. *Angew. Chem. Int. Ed. Engl.* **2009**, *48*, 219–223.

(22) Teschome, B.; Facsko, S.; Schönherr, T.; Kerbusch, J.; Keller, A.; Erbe, A. Temperature-Dependent Charge Transport through Individually Contacted DNA Origami-Based Au Nanowires. *Langmuir* **2016**, *32*, 10159–10165.

(23) Schreiber, R.; Kempter, S.; Holler, S.; Schüller, V.; Schiffels, D.; Simmel, S. S.; Nickels, P. C.; Liedl, T. DNA origami-templated growth of arbitrarily shaped metal nanoparticles. *Small* **2011**, *7*, 1795–1799.

(24) Liu, J.; Geng, Y.; Pound, E.; Gyawali, S.; Ashton, J. R.; Hickey, J.; Woolley, A. T.; Harb, J. N. Metallization of branched DNA origami for nanoelectronic circuit fabrication. *ACS Nano* **2011**, *5*, 2240–2247.

(25) Schreiber, R.; Do, J.; Roller, E.-M.; Zhang, T.; Schüller, V. J.; Nickels, P. C.; Feldmann, J.; Liedl, T. Hierarchical assembly of metal nanoparticles, quantum dots and organic dyes using DNA origami scaffolds. *Nat. Nanotechnol.* **2014**, *9*, 74–78.

(26) Uprety, B.; Gates, E. P.; Geng, Y.; Woolley, A. T.; Harb, J. N. Site-specific metallization of multiple metals on a single DNA origami template. *Langmuir* **2014**, *30*, 1134–1141.

(27) Richter, J.; Seidel, R.; Kirsch, R.; Mertig, M.; Pompe, W.; Plaschke, J.; Schackert, H. K. Nanoscale palladium metallization of DNA. *Adv. Mat.* **2000**, *12*, 507–+.

(28) Tian, C.; Cordeiro, M. A. L.; Lhermitte, J.; Xin, H. L.; Shani, L.; Liu, M.; Ma, C.; Yeshurun, Y.; DiMarzio, D.; Gang, O. Supra-Nanoparticle Functional Assemblies through Programmable Stacking. *ACS Nano* **2017**,

(29) Richter, J.; Mertig, M.; Pompe, W.; Mönch, I.; Schackert, H. K. Construction of highly conductive nanowires on a DNA template. *Appl. Phys. Lett.* **2001**, *78*, 536–538.

(30) Lund, J.; Dong, J.; Deng, Z.; Mao, C.; Parviz, B. A. Electrical conduction in 7 nm wires constructed on λ-DNA. *Nanotechnology* **2006**, *17*, 2752.

(31) Geng, Y.; Pearson, A. C.; Gates, E. P.; Uprety, B.; Davis, R. C.; Harb, J. N.; Woolley, A. T. Electrically conductive gold- and copper-metallized DNA origami nanostructures. *Langmuir* **2013**, *29*, 3482–3490.

(32) Pearson, A. C.; Liu, J.; Pound, E.; Uprety, B.; Woolley, A. T.; Davis, R. C.; Harb, J. N. DNA origami metallized site specifically to form electrically conductive nanowires. *J. Phys. Chem. B* **2012**, *116*, 10551–10560.

(33) Park, S. H.; Prior, M. W.; LaBean, T. H.; Finkelstein, G. Optimized fabrication and electrical analysis of silver nanowires templated on DNA molecules. *Appl. Phys. Lett.* **2006**, *89*, 033901.

(34) Harnack, O.; Ford, W. E.; Yasuda, A.; Wessels, J. M. Tris(hydroxymethyl)phosphine-capped gold particles templated by DNA as nanowire precursors. *Nano Lett.* **2002**, *2*, 919–923.

(35) Uprety, B.; Westover, T.; Stoddard, M.; Brinkerhoff, K.; Jensen, J.; Davis, R. C.; Woolley, A. T.; Harb, J. N. Anisotropic Electroless Deposition on DNA Origami Templates To Form Small Diameter Conductive Nanowires. *Langmuir* **2017**, *33*, 726–735.

(36) Wong, K. K.; Mann, S. Biomimetic synthesis of cadmium sulfide-ferritin nanocomposites. *Adv. Mat.* **1996**, *8*, 928–932.

(37) Balci, S.; Hahn, K.; Kopold, P.; Kadri, A.; Wege, C.; Kern, K.; Bittner, A. M. Electroless synthesis of 3 nm wide alloy nanowires inside Tobacco mosaic virus. *Nanotechnology* **2012**, *23*, 045603.

(38) Sun, W.; Boulais, E.; Hakobyan, Y.; Wang, W. L.; Guan, A.; Bathe, M.; Yin, P. Casting inorganic structures with DNA molds. *Science* **2014**, *346*, 1258361.

(39) Helmi, S.; Ziegler, C.; Kauert, D. J.; Seidel, R. Shape-controlled synthesis of gold nanostructures using DNA origami molds. *Nano Lett.* **2014**, *14*, 6693–6698.

(40) Ding, B.; Deng, Z.; Yan, H.; Cabrini, S.; Zuckermann, R. N.; Bokor, J. Gold nanoparticle self-similar chain structure organized by DNA origami. *J. Am. Chem. Soc.* **2010**, *132*, 3248–3249.

(41) Zhao, Z.; Jacovetty, E. L.; Liu, Y.; Yan, H. Encapsulation of gold nanoparticles in a DNA origami cage. *Angew. Chem. Int. Ed. Engl.* **2011**, *50*, 2041–2044.

(42) Stahl, E.; Martin, T. G.; Praetorius, F.; Dietz, H. Facile and scalable preparation of pure and dense DNA origami solutions. *Angew. Chem. Int. Ed.* **2014**, *53*, 12735–12740.

(43) Seol, S. K.; Kim, D.; Jung, S.; Chang, W. S.; Kim, J. T. One-step synthesis of PEG-coated gold nanoparticles by rapid microwave heating. *J. Nanomat.* **2013**, *2013*.

(44) Morris, J.; Coutts, T. Electrical conduction in discontinuous metal films: A discussion. *Thin Solid Films* **1977**, *47*, 3 – 65.

(45) Barwinski, B. Temperature dependence of electrical conduction in discontinuous gold films on sapphire substrates. *Thin Solid Films* **1985**, *128*, 1 – 9.

(46) Brust, M.; Bethell, D.; Kiely, C. J.; Schiffrin, D. J. Self-Assembled Gold Nanoparticle Thin Films with Nonmetallic Optical and Electronic Properties. *Langmuir* **1998**, *14*, 5425–5429.

(47) Douglas, S. M.; Marblestone, A. H.; Teerapittayanon, S.; Vazquez, A.; Church, G. M.; Shih, W. M. Rapid prototyping of 3D DNA-origami shapes with caDNAno. *Nucleic Acids Res.* **2009**, *37*, 5001–5006.

(48) Ke, Y.; Douglas, S. M.; Liu, M.; Sharma, J.; Cheng, A.; Leung, A.; Liu, Y.; Shih, W. M.; Yan, H. Multilayer DNA origami packed on a square lattice. *J. Am. Chem. Soc.* **2009**, *131*, 15903–15908.

(49) Hill, H. D.; Mirkin, C. A. The bio-barcode assay for the detection of protein and nucleic acid targets using DTT-induced ligand exchange. *Nat Protoc* **2006**, *1*, 324–336.

For TOC only